V European Conference on Computational Fluid Dynamics
ECCOMAS CFD 2010
J. C. F. Pereira and A. Sequeira (Eds)
Lisbon, Portugal,14-17 June 2010

A VISCOUS INVERSE DESIGN METHOD FOR INTERNAL AND EXTERNAL FLOW OVER AIRFOILS USING CFD TECHNIQUES

Raja Ramamurthy*, Benedikt Roidl* and Wahid Ghaly*

*Concordia University
1455 de Maisonneuve, West
MIE Dept, EV 4.151
Montreal, Quebec, CANADA H3G 1M8
e-mail: ghaly@encs.concordia.ca

Key words: Inverse shape design, viscous inverse design, airfoil design, CFD, ALE formulation, aerodynamic blade design, virtual wall movement, finite volume method

Abstract. *An inverse shape design method is developed for steady, two dimensional viscous internal and external flow over airfoils. In this method, a target pressure distribution is prescribed on the airfoil suction side as well as the airfoil thickness distribution. The approach is fully consistent with the viscous flow assumption and is incorporated into the time accurate solution of the Reynolds-Averaged Navier Stokes equations. The latter are expressed in an arbitrary Lagrangian-Eulerian form so as to allow for the airfoil shape to deform according to a virtual wall velocity that is computed from the difference between the current and target pressure distributions. This virtual velocity drives the airfoil to a new shape that would asymptotically produce the prescribed pressure distribution. A cell-vertex finite volume scheme of the Jameson type is used for spacial discretization, and time integration is performed via a dual time stepping. Baldwin-Lomax turbulence model is used for turbulence closure. The inverse method is first validated, it is then used to redesign airfoils for internal and external flow cases. The robustness and usefulness of the inverse method are demonstrated.*

1 INTRODUCTION

Simulating the flow using the Reynolds-averaged Navier Stokes (RANS) equations is now a common tool for determining quantitatively the flow physics and properties in many industrial applications. In the aerospace industry it is used to simulate the flow over airplane wings as well as the flow inside the passages of gas turbine components. State of the art CFD methods are now being used to analyze the performance of almost all parts of e.g airplanes or gas turbines. There are also design methodologies that can be used to improve the performance of a given wing or a given compressor or turbine.

Two-dimensional inverse design methods date back several decades and have been under implementation and continuous development. Historically, inverse methods were developed assuming potential flow, then inviscid but rotational flow and finally assuming viscous flow. Due to this evolution, almost all inverse approaches used today for wings (external flow) or blades (internal flow) contain some traces of inviscid flow implementation such as e.g. the tangency condition which requires that the flow be tangent to the airfoil surface. Moreover, most approaches do not take account of the airfoil motion in the numerical computations, i.e. when the airfoil shape (hence the mesh) is modified, the flow variables are transposed to the new mesh without accounting for this motion in the momentum fluxes across the control volumes nor do they take account of time variation. These observations can be verified by checking the design methods that were reviewed by Dulikravich [1].

For internal flow applications, the inverse blade design methods for viscous flows were shown to be quite efficient [2, 3, 4, 5, 6], however they still carry some traces of inviscid flow implementation. Some methods [2] involve viscous-inviscid interaction (so that the metal profile has to be obtained by subtracting the displacement thickness), some [4, 5] use the tangency condition to find the new blade camberline, while other methods [3] use the transpiration approach where a velocity tangent to the blade is needed. The most recent approach of de Vito *et al.* [6] consists of blending a Navier-Stokes solver, for the flow analysis, with an Euler solver for the inverse design. In all the preceding methods, it is assumed that the flow is attached and the boundary layers are well behaved, so that a representative velocity at the edge of the boundary layer can be used to get the new blade profile. An example presented recently of the use of inverse methods in the design of a multistage compressor to improve stage matching is given in van Rooij *et al.* [7].

Most inverse design methods solve the problem as a time-marching (quasi-steady) problem and do not account for the blade movement in the problem formulation. The errors resulting from the quasi-steady assumption will propagate into the new blade shape which will affect the pressure field computed at the next iteration. In some design approaches and for some target pressure distributions, such errors can result in an inaccurate blade shape or in the divergence of the iterative process. A possible example of this situation is the work of Yang and Ntone [8], who extended the work of Thompkins and Tong [9, 10] to viscous flow, where the blade shape obtained for subsonic viscous flow was rather wavy.

Moreover that approach [8] was not successful in designing transonic blades. The elimination of these errors by using a time accurate formulation will result in a more robust method that can handle relatively 'difficult' design cases. This fact is verified in part by Demeulenaere *et al.* [3] who used a time marching (but not time accurate) approach where they accounted for the mesh movement into the formulation, thus improving the convergence of the inverse method. The merits of using a time accurate solution on a moving and deforming mesh were demonstrated by Daneshkhah and Ghaly [11] who showed that the conventional quasi-steady formulation fails to converge particularly for transonic cases while the time accurate formulation converged without any problems.

The inverse blade design method that was recently developed and presented by Daneshkhah and Ghaly [12, 11] is fully consistent with the viscous flow assumption. The main features of that inverse method are: a- The airfoil walls move with a virtual velocity distribution derived from the difference between the current and the target pressure distributions on the blade surfaces; b- The method is implemented into the time accurate solution of the Reynolds-Averaged Navier-Stokes (RANS) equations, written for a moving and deforming computational domain.

The trends observed for external flow inverse design are similar to those observed in internal flow inverse design particularly that, although these methods are quite efficient, however they still carry some traces of inviscid flow implementation. Some methods use viscous-inviscid interaction [2, 13, 14], some combine viscous analysis with inviscid inverse [15, 16].

In this work, the method originally developed by Daneshkhah and Ghaly [12, 11] and applied to internal flow is extended to external flow and an additional choice of design variables is introduced. The CFD approach is assessed, the inverse design approach is validated and examples of airfoil redesign in internal and external flow are presented. Emphasis is put on the robustness, flexibility and generality of the method in handling different flow configurations and different flow regimes.

2 FLOW GOVERNING EQUATIONS

The Reynolds-averaged Navier-Stokes (RANS) equations are used to describe the flow field (either external or internal) both in the analysis and in the design modes of the computations. The RANS equations are written in the Arbitrary Lagrangian-Eulerian (ALE) form to take account of the moving and deforming mesh (in the design approach). The conservative form of the governing equations for unsteady two-dimensional flow is written as:

$$\frac{\partial \mathbf{U}}{\partial t} + \frac{\partial (\mathbf{F} - \mathbf{F}_g - \mathbf{F}_v)}{\partial x} + \frac{\partial (\mathbf{G} - \mathbf{G}_g - \mathbf{G}_v)}{\partial y} = 0 \tag{1}$$

where U is the vector of conservative flow variables, $\mathbf{F} - \mathbf{F}_g$ and $\mathbf{G} - \mathbf{G}_g$ are the convective flux vectors relative to the moving grid, and $\mathbf{F}_v$ and $\mathbf{G}_v$ are the viscous flux vectors.

They are discretized in space using a second order cell-vertex finite volume method of Jameson's type on a fully unstructured triangular mesh [17]. The method uses an explicit

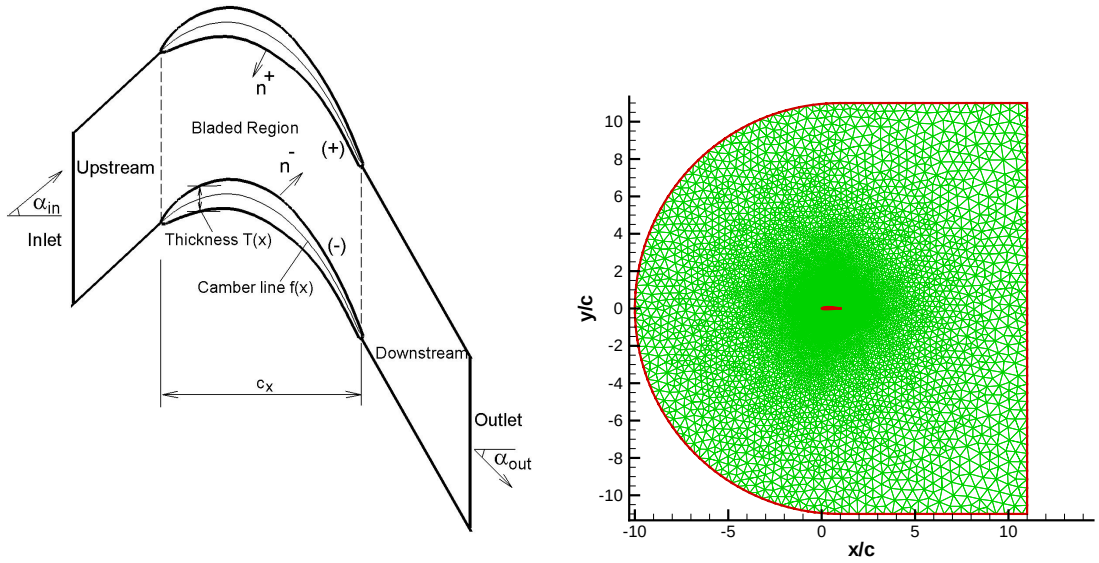

Figure 1: Computational domain for a turbine cascade (left) and for an isolated airfoil (right).

Runge-Kutta pseudo-time stepping procedure to obtain the stationary solution where local pseudo-time stepping and implicit residual smoothing are employed for convergence acceleration. During the design process, a time accurate solution is ensured using a dual time stepping scheme [18]. The grid velocities for a moving mesh are computed from the space conservation law (SCL) [19]. The Baldwin-Lomax model [20], adapted for the use on unstructured meshes [21] is used for turbulence closure.

For external flow applications, the farfield boundary condition is obtained from the Riemann invariants and the no slip condition is applied on the airfoil surface. For internal flow in a two-dimensional cascade of blades, the inlet total pressure and temperature and the flow angle at inlet and the static pressure at exit are specified. The flow is assumed periodic between adjacent blade passages so that one blade passage is simulated with periodic boundary conditions between adjacent passages. The cascade notation and computational domain for a turbine cascade are given in Fig. 1; the same notation is used for airfoils in external flow. The computational domain for the flow over an isolated airfoil is given in Fig. 1.

3 INVERSE DESIGN METHOD

Since both internal and external flows are governed by the same equations then the same inverse design method applies to both. The current approach is to replace the fixed-wall boundary condition with a moving-wall boundary condition; this movement is controlled by a virtual velocity distribution $\mathbf{v} = (u^v, v^v)$ that arises from the difference between the current and the prescribed target pressure distributions [9]. This transient velocity is

derived from the momentum flux balance between the target pressure distribution on the target non-moving airfoil and the current transient pressure distribution on a moving and deforming airfoil.

The transient convective momentum flux **F** on the airfoil surface that is moving with a virtual velocity distribution has the following form [11]:

$$\mathbf{F} = \begin{bmatrix} (\rho u^v u^v + p)\, n_x + (\rho u^v v^v)\, n_y \\ (\rho u^v v^v)\, n_x + (\rho v^v v^v + p)\, n_y \end{bmatrix} \tag{2}$$

where $\mathbf{n} = (n_x, n_y)$ is the vector normal to the airfoil surface. When the airfoil reaches the target shape (that corresponds to the target pressure distributions), the virtual velocities asymptotically reach zero and thereby the target momentum flux yields

$$\mathbf{F^d} = \begin{bmatrix} (p^d n_x) \\ (p^d n_y) \end{bmatrix} \tag{3}$$

By equating the transient and the target momentum fluxes, Eqs. 2 and 3, the virtual velocity components in the x- and y-directions are found.

$$\begin{aligned} v^v &= \pm \left(\frac{n_y^2}{n_x^2 + n_y^2} \frac{|p^d - p|}{\rho} \right)^{\frac{1}{2}} \\ u^v &= v^v \frac{n_x}{n_y} \end{aligned} \tag{4}$$

The sign of the virtual velocities is chosen such that positive virtual velocities exist when there is positive pressure difference between target and current pressures and vice versa. For convenience, the wall motion is taken normal to the airfoil surface and which is computed as

$$v_n^v = \mathbf{v}^v \cdot \mathbf{n} \tag{5}$$

It is required that the virtual velocities computed be under-relaxed so as to ensure the problem stability [9]. This under-relaxation factor is expressed as

$$\omega = \varepsilon \cdot (1/a)\sqrt{|\Delta p|/\rho} \tag{6}$$

where a is the speed of sound and ε is a constant that varies between 0.1 and 0.2 for subsonic flow cases and about 0.05 for transonic flow cases.

The wall displacement δs is proportional to v_n^v, but is in the opposite direction so as to counter this virtual velocity and thereby driving it to zero. Therefore $\delta s = (\delta x, \delta y)$ is given as,

$$\delta s = -\omega\ v_n^v\ \delta t \tag{7}$$

where δt is the user defined physical time step. The modified airfoil geometry is then constructed by applying wall displacement on discrete airfoil points i.e.

$$x_{new} = x_{old} + \delta x$$
$$y_{new} = y_{old} + \delta y \tag{8}$$

It is interesting to note that the present inverse formulation works well for inviscid as well as viscous flows although, in Eq. 2, the viscous flux terms were neglected, and the balance of convective flux terms only was used to move the walls towards a shape that would satisfy the target pressure distribution [22]. It is believed that this is due to the fact that all the studied cases correspond to high Reynolds number flows where the viscous fluxes are negligible compared with the convective fluxes.

3.1 Design Variables

In the current implementation, two choices of design variables are proposed. Choice 1 consists of prescribing the pressure distributions on both pressure and suction surfaces; the airfoil geometry is then driven by the difference between the target and the current pressure distributions along the airfoil surfaces.

Choice 2 consists of prescribing the suction surface pressure distribution and the airfoil thickness distribution. This option is practical for airfoil design since the suction side pressure distribution predominantly dictates the airfoil performance; it gives more control on the flow over the airfoil and hence on the performance so that e.g. weakening of a shock or reducing a flow separation region can be achieved through the choice of p^-. Since the pressure surface pressure distribution has little impact on the flow, the pressure from the current time step is used as the design target. The thickness distribution ensures that the airfoil is closed and allows for satisfying manufacturing and structural constraints.

3.2 Inverse Design Implementation

The airfoil movement is represented schematically in Fig. 2. The resulting airfoil is scaled back to the original chord length. The discrete x-location points are interpolated back to their original x-location, thereby the airfoil is essentially moving only in y-direction. The new camberline and thickness are now computed from the modified geometry as

$$f(x)_{new} = 0.5(y(x)^-_{(new)} + y(x)^+_{(new)}) \tag{9}$$

$$T(x)_{new} = y(x)^-_{(new)} - y(x)^+_{(new)} \tag{10}$$

The resulting camberline profile is smoothed to eliminate any geometry oscillation using the following elliptic form:

$$f_j = f_j + \omega_s[|f_{j+1} - f_j|(f_{j+1} - f_j) + |f_{j-1} - f_j|(f_{j-1} - f_j)] \tag{11}$$

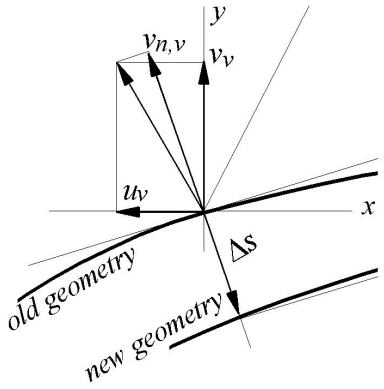

Figure 2: Schematic representation of wall movement

where j refers to the discrete points on the airfoil camberline. A typical value for the smoothing coefficient ω_s is 0.2 for subsonic flow cases and is 0.05 for transonic cases. It is also recommended to modify the smoothing coefficient with the amount of displacement δs. When p^- and $T(x)$ are prescribed, Choice 2, the new p^- and p^+ are generated by adding the prescribed thickness distribution to the new smoothed camberline as follows:

$$y(x)^{\pm}_{new} = f(x)_{new} \pm 0.5T(x)_{prescribed} \tag{12}$$

For Choice 1, where p^+ and p^- are the design variables, it is suggested that the thickness distribution be smoothed in a similar manner (Eq. 11) as camberline smoothing before computing the camberline (Eq. 9) so as to ensure a smooth distribution, and depending upon the case, camberline smoothing may be eliminated. The new geometry is constructed by adding the new thickness to the new camberline.

$$y(x)^{\pm}_{new} = f(x)_{new} \pm 0.5T(x)_{new} \tag{13}$$

After the new geometry is obtained, the design constraints are enforced, as detailed in the next section, to get the final shape.

The next step is to displace the computational grid according to the wall movement. This is presently done by using transfinite interpolation as it has the ability to displace the grid at a relatively low computational cost. From this grid movement, the grid velocities are calculated using the Space Conversation Law (SCL) which are in turn substituted into the flow governing equations (Eq. 1).

3.3 Design Constraints

An arbitrary choice of target pressure distribution does not necessarily mean that the inverse design problem is well posed. As described by Mangler W. [23], Lighthill M.J.

[24] and later by Volpe *et al.* [25], there are three integral constraints relating target pressures and free stream conditions that need to be satisfied to ensure a well posed problem. Otherwise we may end up with a trailing edge crossover, an open airfoil, or any unrealistic airfoil configuration. In the present implementation this is taken care of by solving the inverse problem between $0.5\% - 2\%$ and $98\% - 99.5\%$ of the chord while the remaining parts which fall near the leading and trailing edges are solved in analysis mode. To ensure the profile smoothness at the transition points, the slope of the camberline and the airfoil thickness are matched with those prevailing from the design region.

3.4 Inverse Design Algorithm

Figure 3 shows the inverse design iterative process. The design module starts from a semi-converged or a fully converged solution on an initial geometry where the target pressures are read. The difference between the target and the current design pressures are used to compute the virtual velocities. The virtual wall velocities are then translated into displacements that are used to modify the airfoil shape. The next step is to adjust the computational grid using transfinite interpolation. The grid velocities are computed from Space Conservation Law [19]. The grid velocities are added on to the governing equations and the stationary problem is solved until the residuals reach a predetermined convergence level. The design and target pressures are compared and the whole process is repeated until the L_2 norm of the grid displacements are within the tolerance value; this ensures that the airfoil is not moving and steady state condition is asymptotically reached.

4 ASSESSMENT, VALIDATION AND REDESIGN OF THE RAE 2822 AIRFOIL

To assess the accuracy of the CFD method, the computer program is run in analysis mode for the RAE 2822 airfoil at transonic flow conditions and the results thus obtained are compared with the available experimental data. The inverse design method is then validated by imposing the original pressure distribution of one airfoil as target but starting the design from a different airfoil geometry. Last but not least, the inverse method is used to redesign the RAE 2822 airfoil.

4.1 Assessment of the CFD method

The flow analysis method is assessed for its accuracy by comparing the computed lift and drag coefficients against the experimental values for the RAE 2822 airfoil. The inverse design method is then validated by imposing the original pressure distribution of one airfoil as target but starting the design from a different airfoil geometry.

A hybrid mesh was employed on the computational domain that consists of a C-mesh where the far-field boundary is taken at 10 chords away from the airfoil. Near the airfoil, a structured and stretched O-mesh of rectangles that are cut into triangles surrounds

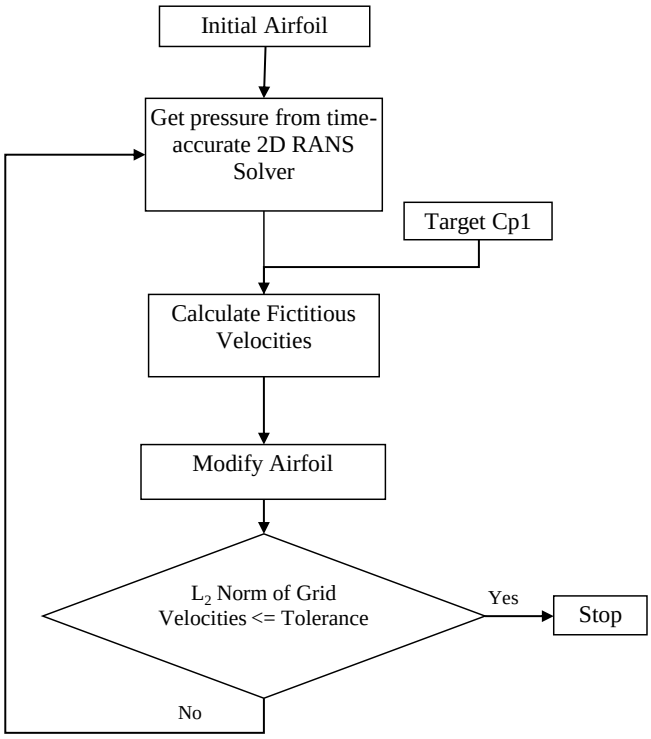

Figure 3: Computation algorithm for inverse design

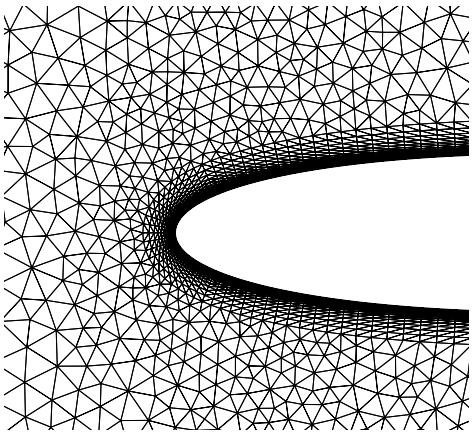

Figure 4: Mesh close-up near airfoil leading edge

Table 1: Analysis Method Assessment

Case	Lift coefficient (c_l)		Drag coefficient (c_d)	
	Computed	Experimental	Computed	Experimental
RAE 2822	0.782	0.743	0.0111	0.0127

the airfoil so as to resolve the boundary layer while the rest of the domain is filled with Delaunay triangulation. A $y^+ < 1$ was maintained at the first node away from the wall. The domain consisted of 17414 nodes (34447 cells). A close up of the mesh near the leading edge is shown in Fig. 13. A background mesh as required by the turbulence model was created with entirely unstructured mesh with rays going normally outwards from the airfoil surface and has 17153 nodes (33620 cells).

The transonic flow over the RAE 2822 airfoil is analyzed at $M_\infty = 0.725, \alpha = 2.92°, Re =$ 6.5 millions, see AGARD AR 138 section A-6, test case 6 [26]. For this case, there is a transonic bubble on the suction side and a shock is observed between 50% and 60% chord. The computed lift and drag coefficients are compared with the experimental values in Table 1. The computed and experimental values of pressure coefficient are given in Fig. 5.

4.2 Validation of the inverse method

The viscous inverse design method is verified by inversely designing an existing airfoil (referred to as target), where the airfoil design variables are prescribed. The validation case is that of recovering a NACA 0012 airfoil starting from an RAE 2822 airfoil; the flow

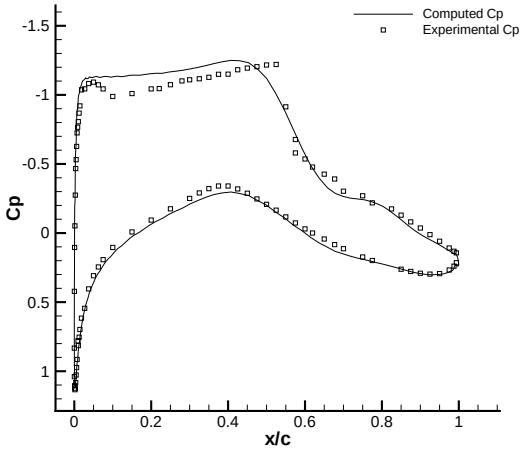

Figure 5: Assessment of CFD - Computed Vs Experimental Cp values for RAE 2822 airfoil

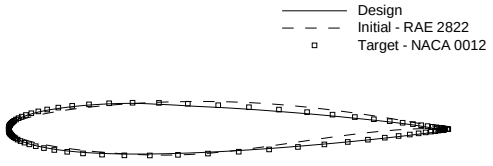

Figure 6: Inverse Design validation - Initial, target and design airfoil geometry

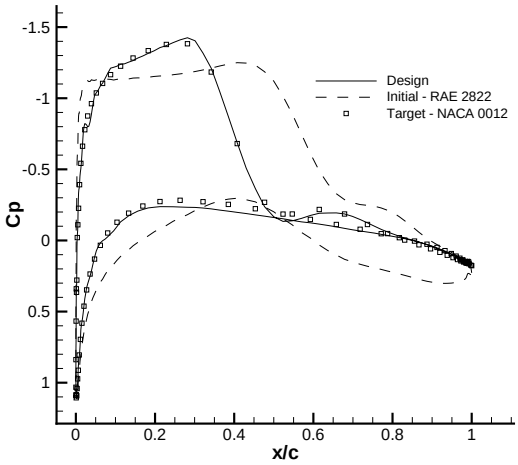

Figure 7: Inverse Design validation - Initial, target and design Cp plot

Table 2: Design Method Validation for RAE 2822 to NACA 0012, $M_{inf} = 0.725, AOA = 2.92°, Re = 6.5$ millions

Lift coefficient (c_l)		Drag coefficient (c_d)	
Design	Target	Design	Target
0.466	0.444	0.0164	0.0134

being transonic over both airfoils. For the inverse design process, NACA 0012 airfoil was analyzed under the same flow conditions where a shock appears on the suction side and is located between 30% and 40% chord. Inverse design was started from a fully converged solution of the RAE 2822 airfoil and the pressure distributions on pressure and suction surfaces of NACA 0012 were applied as target. The final airfoil shape corresponding to NACA 0012 was achieved in around 1200 design steps where the L_2 norm of grid displacements went down to 2×10^{-4}. The number of design iterations is higher than that of a subsonic flow case as the under-relaxation factors were kept low in order to maintain the problem stability and eliminate any waviness that may occur in the shock region. Figures 6 and 7 show the initial, target and design airfoil geometries and Cp distributions, respectively. The design values of c_l and c_d are compared with the target values in Table 2; given that this is a transonic case, the agreement is rather fair.

4.3 Inverse design of a NACA 2412 airfoil in transonic flow

The inverse design method is used to redesign a NACA 2412 in transonic flow. The method robustness, flexibility and usefulness in designing airfoils in viscous subsonic and

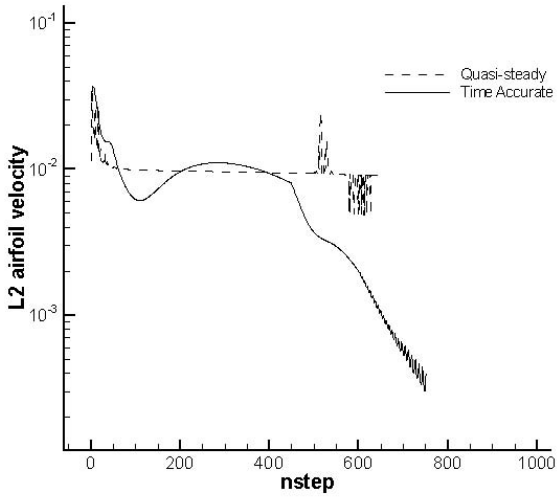

Figure 8: NACA 2412 redesign: design convergence history.

transonic flows are demonstrated.

In order to demonstrate the benefits of using a time-accurate simulation on a moving mesh and to describe the evolution of the blade shape from the initial guess to the final steady shape, the design approach was carried out using the time-accurate and the quasi-steady approaches. The former approach does not account for the mesh movement during the design solution and a steady-state solution is assumed for the flow field after each airfoil shape modification. Figure 8 compares the convergence history of the time-accurate with the quasi-steady simulations, where the latter did not converge and failed to recover the airfoil geometry and the target pressure distribution. A similar convergence behavior was also observed when designing a compressor blade in internal transonic flow, see Fig. 9.

The main aim of this redesign case is to apply the inverse method to a separated flow case in an attempt to reduce the separated flow region. NACA 2412 was analyzed at an AOA of 12°, Mach of 0.39 and Reynolds number of 2.6 millions. Target Cp was tailored such that the flow possesses higher energy upstream of the separation region so as to energize the low momentum fluid near the wall and reduce the separation region, hence increasing c_l. Also the peak of the target Cp near the leading edge was reduced in magnitude thereby reducing the pressure recovery and hence delaying separation. Reduction of peak Cp also leads to lower mach numbers, and transonic flow or a weak shock near the leading edge region could be eliminated and thereby reducing losses.

The design was carried out at relatively low relaxation factors due to the presence of a small transonic region near the airfoil leading edge which led to relatively slow but stable convergence rate. After 920 design iterations the target Cp distribution was reached; Fig. 10 shows the initial, target and design isentropic Mach number distributions. It is seen that the transonic bubble near the leading edge was reduced and almost matches with the

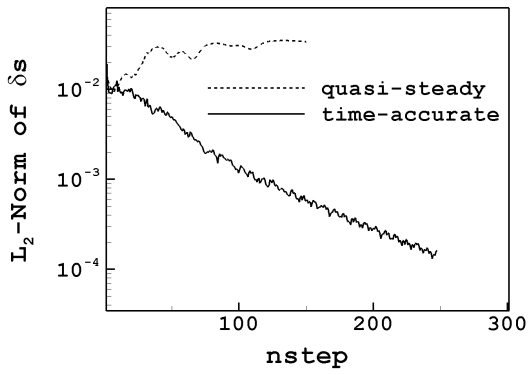

Figure 9: Transonic compressor: design convergence history, [11].

Table 3: Redesign of NACA 2412 airfoil: $M_{inf} = 0.39, AOA = 12°, Re = 2.6$ millions

Lift coefficient (c_l)		Drag coefficient (c_d)		Lift/Drag (c_l/c_d)	
*D*esign	Original	Design	Original	Design	Original
1.392	1.250	0.0437	0.0517	31.805	24.158

target. The small deviation could be attributed to retaining the shape of the leading edge which is enforced as a constraint in the first couple of percents. However, the leading edge did change its orientation so as to match the target. As intended, the size and extent of the separation region are reduced, as seen in Fig. 12. The original and designed airfoil profiles are shown in Fig. 11. The design and original values of c_l and c_d given in Table 3, show an increase in c_l and a decrease in c_d.

5 ASSESSMENT, VALIDATION AND REDESIGN OF A TURBINE CASCADE

The LS89 transonic turbine vane, which is designed and tested at the von Karman Institute [27], is selected as a test case to assess and demonstrate the capability and usefulness of the present inverse design scheme.

The inverse design simulation code is first run in analysis mode and the results thus obtained are compared with the LS89 experimental data so as to assess the reliability and accuracy of the CFD method. The inverse design method is then assessed for its robustness and accuracy by inverse designing the LS89 using its original pressure distribution as target but starting from a different blade geometry. The inverse method is then applied to redesign the LS89 blade profile in order to achieve a modified target pressure distribution.

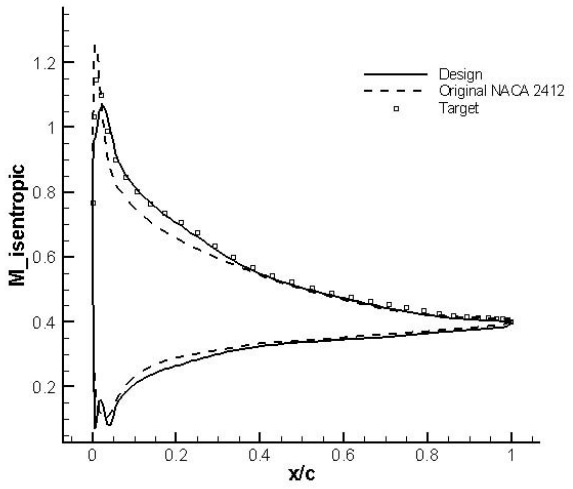

Figure 10: Redesign of NACA 2412: Original, target and design Cp distributions

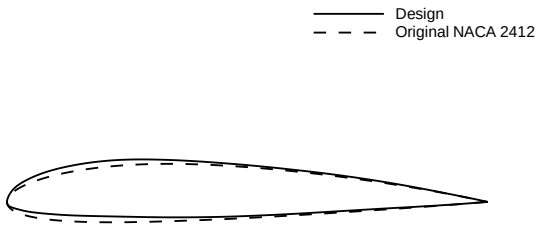

Figure 11: Redesign of NACA 2412: Original and redesigned airfoil geometry

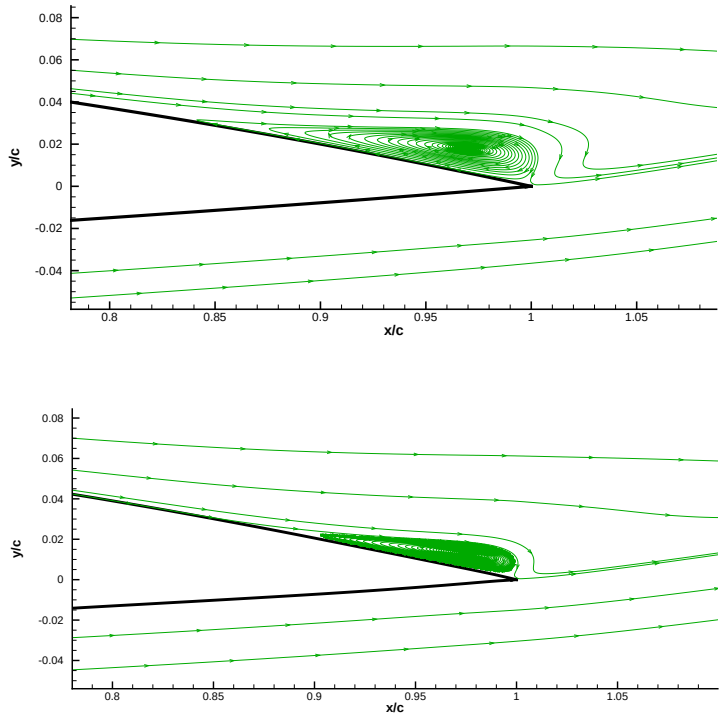

Figure 12: Redesign of NACA 2412: Recirculation zone on suction surface: Top-Initial, Bottom-Redesigned

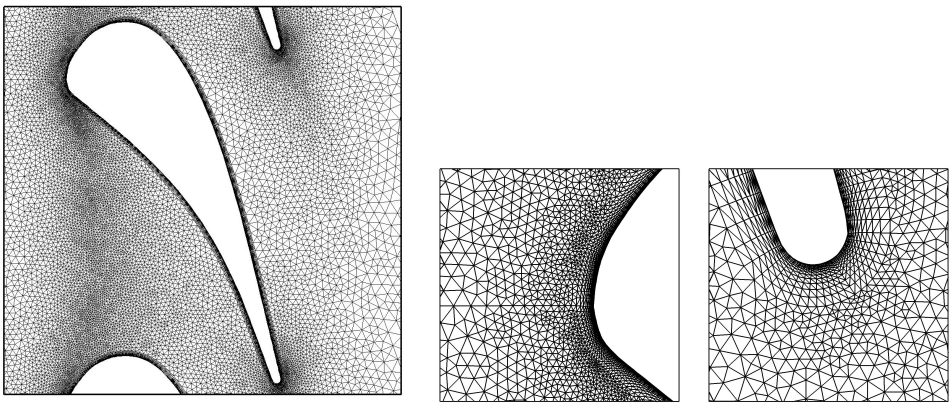

Figure 13: Computational mesh and LE/TE close-up

5.1 Assessment of the analysis scheme

The inverse design simulation method was first run in the analysis mode. The isentropic Mach number distribution thus obtained for a subsonic and a transonic outflow condition are compared with experimental data [27].

Figure 13 shows the unstructured mesh with a close-up of the LE/TE regions. In order to achieve the resolution requirements in the boundary layers, a structured mesh is constructed around blade in such a way that the first point away from the wall results in an average $y^+ < 1$. Figure 14 shows the stream lines at LE/TE regions for the subsonic case which clearly shows the LE stagnation point and TE vortices.

Figure 15 shows a comparison of measured and computed blade isentropic Mach number distributions along the blade surfaces for $M_{2is} = 0.875$ and $M_{2is} = 1.02$ cases with $Re = 10^6$. The agreement is very good for the subsonic case and fair for the transonic case. There are some discrepancies on the suction side near the shock location for the transonic case. The reason maybe attributed to laminar to turbulent transition occurring in the experiment at the rear part of the blade suction side and to some related unsteady effects [27].

5.2 Assessment of the inverse design method

In this section, the viscous inverse design method is verified by inversely designing the LS89 blade for the subsonic outflow condition ($M_{2is} = 0.875, Re = 10^6$) using its original pressure distribution as the design target. The initial geometry is the same profile as LS89, but rotated by 2° in the clockwise direction, as depicted in Fig. 16.

The initial and target geometries are first analyzed by solving the RANS equations using the same code but in analysis mode. The resulting blade pressure distributions are presented in Fig. 17. As it is shown by de Vito et. al. [6], in order to obtain a unique inverse solution, one has to specify the blade mass flow rate. This is accomplished

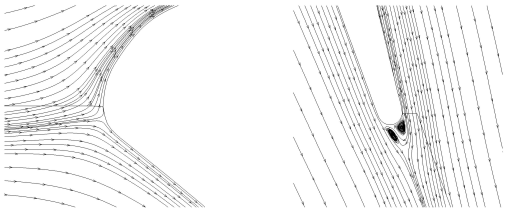

Figure 14: Close-up of streamlines at LE/TE

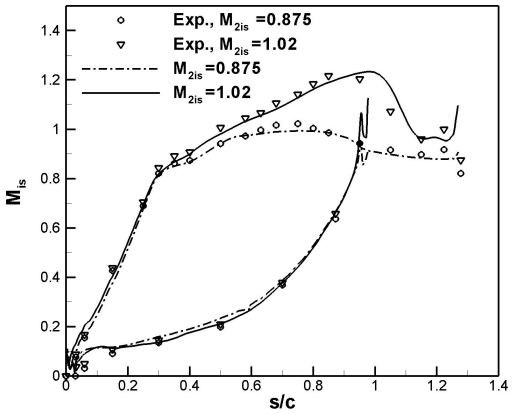

Figure 15: Isentropic Mach no. distributions

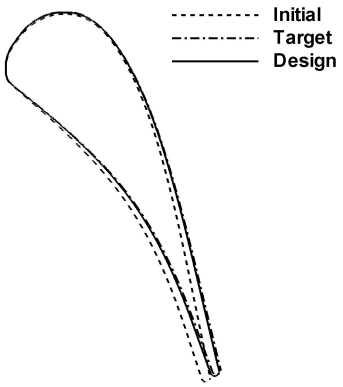

Figure 16: Original,initial and designed LS89 blade

indirectly by adjusting the back pressure until the target mass flow rate is reached. In practice this could be done every 3-5 iterations during the inverse design solution and modifications are reduced when the mass flow rate is approaching the target. A similar approach is adapted in the present work. The difference in the computed and target reduced mass flow rate using this approach is less than 0.2% for this case.

The resulting blade pressure distributions using the inverse method are given in Fig. 17, which shows that the target distribution was achieved, rather accurately. Figure 16 shows that the target blade profile is very well recovered by the design method. The original geometry is recovered after about 400 geometry modification steps. The time-accurate solution which is obtained after each geometry modification step requires about 200 iterations to converge the local problem (no multigrid approach was used) and the number of iterations are reduced as the design approaches the target. The overall computation time is equivalent to that of 4 analysis calculations.

5.3 Redesign of the LS89 transonic vane

The inverse design method was applied to the redesign of the highly loaded transonic vane VKI-LS89 at transonic outflow conditions where the isentropic exit Mach numbers is $M_{2,is} = 1.02$.

The design variables were chosen to be the pressure distributions on both pressure and suction surfaces of the vane; the original and target pressure distributions are given in Fig. 18. The target pressure distribution on the pressure side was chosen to be the same as the one prevailing from analysis of the original vane as the flow was found to be insensitive to almost any modification in pressure on the vane pressure side. The target pressure distribution on the vane suction side was smoothed out in the region between

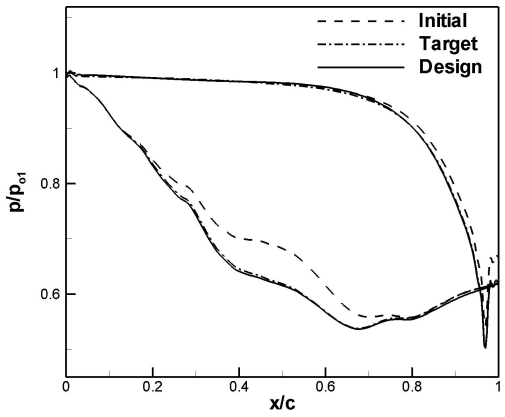

Figure 17: Pressure distributions for design assessment

20% and 70% chord, and the diffusion region which is located at about 85% was reduced. Note that the thickness distribution is not fixed however the 'small' difference between the original and target pressure distributions and the design considerations whereby the first and last 1% of the vane are run in analysis mode ensure that the blade shape is closed and smooth.

The design converged after 500 design steps which is equivalent to 2 analysis simulations, i.e. the difference between the target and computed pressure loading has reached an acceptable tolerance. The latter is measured by the L_2-norm of the grid velocity, which was set to 10^{-4}. A good agreement between target and computed pressure distributions is obtained as depicted in Fig. 18.

The resulting pressure loss coefficient (ζ), mass flux, etc. are presented in Table 4, where ζ is the pressure loss coefficient; it was reduced by 5%. As it is presented in Fig. 19, the required geometry modifications were marginal and geometric parameters such as vane leading and trailing edge radii, and throat did not change. The reduced mass flow rates at the operating conditions varied by 0.26%. This variation is due to the fact that the mass flow rate is fixed indirectly by manually varying the back pressure downstream of the rotor. (The mass flow rate is fixed so as to obtain a unique blade shape [28]).

The pressure ratio varied between the original and design conditions by 0.03%. This variation is due to the fact that the total pressure loading (given by the area under the pressure loading curve) resulting from the target pressure distributions is not exactly equal to the one prevailing in the original vane.

Table 4: VKI-LS89 redesign results

	Original	Design
$\dot{m}_{red.}$	0.2698	0.2705
ζ %	7.14	6.80
PR	1.919	1.920

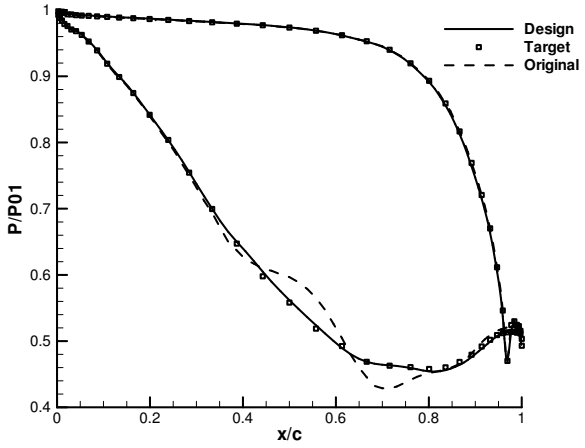

Figure 18: LS89 pressure distributions for transonic outflow conditions

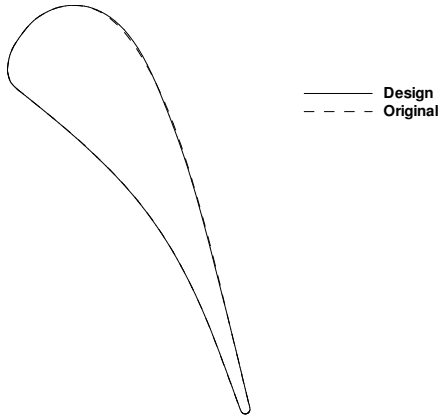

Figure 19: Original and redesigned LS89 blade geometry

6 CONCLUSION

An aerodynamic inverse shape design method is successfully developed for 2D external and internal viscous flows, where the pressure distribution on the airfoil surfaces are chosen as design variables. A virtual wall velocity that is calculated from the difference between the target and current pressure distributions, is used to modify the airfoil geometry. The problem is solved in a time accurate fashion which contributed to convergence acceleration as temporal errors were eliminated. The redesign cases performed especially in transonic flow with flow separation regions confirm the robustness of the methodology implemented in internal as well as external flow.

REFERENCES

[1] Dulikravich, G. S. (1992) Aerodynamic shape design and optimization: Status and trends. *Journal of Aircraft*, **29**.

[2] Giles, M. and Drela, M. (1987) Two dimensional transonic aerodynamic design method. *AIAA Journal*, **25(9)**, 1199–1205.

[3] Demeulenaere, A., Leonard, O., and Van den Braembussche, R. (1997) A two-dimensional navier-stokes inverse solver for compressor and turbine blade dasign. *Proceedings of the Institution of Mechanical Engineers, PART A.*, **211**, 299–307.

[4] Damle, S., Dang, T., Stringham, J., and Razinsky, E. (1999) Practical use of a 3d viscous inverse method for the design of compressor blade. *Journal of Turbomachinery*, **121**, 321–325.

[5] Choo, B. and Zangeneh, M. (2002) Development of an (adaptive) unstructured 2-d inverse design method for turbomachinery blades. *ASME paper GT-2002-30620*.

[6] de Vito, L., den Braembussche, R. V., and Deconinck, M. (2003) A novel two-dimensional viscous inverse design method for turbomachinery blading. *Journal of Turbomachinery*, **125**, 310–316.

[7] van Rooij, M., Dang, T., and Larosiliere, L. (2007) Improving aerodynamic matching of axial compressor blading using a three-dimensional multistage inverse design method. *Journal of Turbomachinery*, **129**, 108–118.

[8] Yang, T. and Ntone, F. (1986) Viscous compressible flow direct and inverse computation with illustration. *NASA-CR-175037*.

[9] Thompkins, W. and Tong, S. (1982) Inverse or design calculation for nonpotential flows in turbomachinery cascades. *ASME Journal of Engineering for Power*, **104**, 281–285.

[10] Tong, S. and Thompkins, W. (1982) A design calculation procedure for shock-free or strong passage shock turbomachinery cascades. *ASME Paper 82-GT-220*.

[11] Daneshkhah, K. and Ghaly, W. (2007) Aerodynamic inverse design for viscous flow in turbomachinery blading. *AIAA Journal of Propulsion and Power*, **23**, 814–820.

[12] Daneshkhah, K. and Ghaly, W. (2006) An inverse blade design method for subsonic and transonic viscous flow in compressors and turbines. *Journal of Inverse Problems in Science and Engineering*, **14**, 211–231.

[13] Gopalarathnam, A. and Selig, M. S. (2001) Low-speed natuaral-laminar-flow airfoils: Case study in inverse airfoil design. *Journal of Aircraft*, **38**, 57–63.

[14] Gopalarathnam, A. and Jepson, J. K. (2005) Inverse design of adaptive airfoils with aircraft performance considerations. *Journal of Aircraft*, **42**.

[15] Hirose, N., Takanashi, S., and Kawai, N. (1987) Transonic airfoil design procedure utilizing a **N**avier-stokes analysis code. *AIAA*, **25**, 353–359.

[16] Malone, J. B., Narramore, J. C., and Sankar, L. N. (1991) Airfoil design method using the navier-stokes equations. *Journal of Aircraft*, **28**, 216–224.

[17] Mavriplis, D., Jameson, A., and Martinelli, L. (1989) Multigrid solution of the navier stokes equations on triangular meshes. *AIAA Paper 89–0120*.

[18] Jameson, A. (1991) Time dependent calculations using multigrid, with application to unsteady flow past airfoils and wings. *AIAA Paper 91–1596*.

[19] Demirdzic, I. and Peric, M. (1988) Space conservation law in finite volume calculations of fluid flow. *International Journal for Numerical Methods in Fluids*, **8**, 1037–1050.

[20] Baldwin, B. and Lomax, H. (1978) Thin layer approximation and algebraic model for separated turbulent flows. *AIAA Paper 78–257*.

[21] Mavripilis, D. (1991) Turbulent flow calculations using unstructured and adaptive meshes. *International Journal for Numerical Methods in Fluids*, **91**, 1131–1152.

[22] Daneshkhah, K. (2007) Aerodynamic inverse design of turbomachinery blading in two-dimensional viscous flow. *Ph.D. Thesis, Concordia University, Department of Mechanical Engineering*.

[23] Mangler, W. (1938) Die berechunung eines traflugelprofiles mit vorgeschriebener druckverteilung. *Jahrbuch der Deutschen Luftfahrtanschung*.

[24] Lighthill, M. J. (1945) A new method of two-dimensional aerodynamic design. *Aeronautical Research Council*.

[25] Volpe, G. and Melnik, R. E. (1986) The design of transonic aerofoils by a well-posed inverse method. *International Journal for Numerical Methods in Engineering*, **22**, 341–361.

[26] Cook, M. M., P.H. and Firmin, M. (1979) Aerofoil rae 2822 - pressure distributions, and boundary layer and wake measurements, experimental data base for computer program assessment. *AGARD-AR-138*.

[27] Arts, T., de Rouvroit, L., and Rutherford, A. (1990) Aero-thermal investigation of a highly loaded transonic linear turbine guide vane cascade. *von Karman Institute for Fluid Dynamics. Technical Note 174*.

[28] Daneshkhah, K. and Ghaly, W. (2007) Redesign of a highly loaded transonic turbine nozzle blade using a new viscous inverse design method. *ASME paper GT2007-27430*.